ISIJ International, Vol. 47 (2007), No. 10, pp. 1436–1443

Design of Swirling Flow Submerged Entry Nozzles for Optimal Head Consumption between Tundish and Mold

Yuichi TSUKAGUCHI,[1,2] Osamu NAKAMURA,[1] Pär JÖNSSON,[3] Shinichiro YOKOYA,[3,4] Toshihiro TANAKA[5] and Shigeta HARA[6]

1) Corporate R&D Labs., Sumitomo Metal Industries, Ltd., 16-1 Sunayama, Kamisu, Ibaraki 314-0255 Japan.
2) Graduate Student, Graduate School of Engineering, Osaka University, 2-1 Yamadaoka, Suita, Osaka 565-0871 Japan.
3) Division of Applied Process Metallurgy, KTH, SE-100 44 Stockholm, Sweden. 4) Nippon Institute of Technology, 4-1 Gakuendai, Miyashiro, Saitama 345-8501 Japan. 5) Graduate School of Engineering, Osaka University, 2-1 Yamadaoka, Suita, Osaka 565-0871 Japan. 6) Formerly Graduate School of Engineering, Osaka University. Now at Emeritus Professor, Graduate School of Engineering, Osaka University, 2-1 Yamadaoka, Suita, Osaka 565-0871 Japan and Department of Mechanical Engineering, Fukui University of Technology, 3-6-1 Gakuen, Fukui 910-5805 Japan.

(*Received on May 22, 2007; accepted on August 17, 2007*)

A technology of swirling flow formation in a submerged entry nozzle is proposed as an effective measure for controlling the flow pattern in a continuous casting mold. As a result of a joint study between Nippon Institute of Technology, Osaka University, Kyushu Refractories, and Sumitomo Metal Industries, swirling flow submerged entry nozzles with a swirl blade for steel slab casting have been developed to improve the productivity of the process and the surface quality of slabs and coils.

The swirl blade in the submerged entry nozzle forms the swirling flow expending the potential energy between the tundish and the mold. Thus, the swirl blade and the internal shape of the submerged entry nozzle, which determine the swirling flow rate, should be designed considering the flow rate in the nozzle and the head between the tundish and the mold of the applied casting machine.

From full-scale water model experiments, we obtained an empirical equation to estimate the required head between the tundish and the mold from the flow rate, the internal shape of the nozzle, and the specification of the swirl blade. Then, we investigated energy efficiency to create the swirling flow, using an empirical equation from the results of a water model experiment and a numerical analysis of the swirling flow in the nozzle.

The obtained empirical equation is valuable to design swirling flow submerged entry nozzles adopted for various casting conditions.

KEY WORDS: continuous casting; submerged entry nozzle; swirling flow; swirl blade; potential energy; head; water model.

1. Introduction

Gas bubbles and non-metallic inclusions must be removed from liquid steel at the meniscus, while the mold wall must be cooled to solidify the steel. This illustrates the fundamental difficulty of continuous casting operations, *i.e.*, the meniscus temperature must be kept high, but the solidified shell is cooled through the mold wall beside the meniscus.

In general, as the temperature on the meniscus is controlled through the flow pattern at the outlet of the submerged entry nozzle, it is important to create a reasonable bulk mold flow controlling the flow pattern at the outlet. To avoid the trapping of gas bubbles and non-metallic inclusions by the solidified shell, there must be a lower limit on the meniscus flow velocity. In addition, an upper limit on the meniscus flow velocity is necessary to prevent the entrapment of mold flux at the meniscus. An appropriate range for meniscus flow velocity is therefore necessary to satisfy those two conditions.[1–3] Overall, it is important to optimize both the velocity and the temperature of the steel in the mold controlling the flow pattern in the mold.

Electromagnetic brakes and electromagnetic stirrers are widely used to control the bulk mold flow pattern.[4–7] However, even if some electromagnetic device is applied, there is a limitation of controlling the flow pattern in the mold because it is difficult to measure the molten steel flow precisely. Therefore, if the outlet flow from submerged entry nozzle fluctuates, it becomes embarrassed to control flow pattern in the mold accurately.

To control the flow in the mold stably, it is important to modify the flow in the submerged entry nozzle as a root measure. From this viewpoint, the creation of a swirling flow in the submerged entry nozzle to control the bulk mold flow has been proposed by Yokoya *et al.*,[8–10] and in 1997, a joint study between Nippon Institute of Technology, Osaka University, Kyushu Refractories, and Sumitomo Metal Industries began to make the best use of 'seed research' in in-

dustrial steel casting.[11,12] The potential energy from a tundish head is used to create a swirling flow when the steel flows past a twist-tape blade inserted into the submerged entry nozzle. In consequence of the development, the submerged entry nozzle with a swirl blade (here referred to as the swirling flow nozzle) helps creating a stable bulk mold flow, which has resulted in improvement of the quality of the product and the productivity of the process without any electromagnetic devices.[13]

As mentioned above, it is necessary to use the potential energy between the tundish and the mold in an optimal manner to achieve a stable mold flow through the swirling flow nozzle. Thus, when designing the swirl blade and the inner shape of the submerged entry nozzle, it is necessary to consider the required head between the tundish and the mold in the applied conditions of the submerged entry nozzle to achieve the optimal swirling flow rate with the suitable head consumption.

The present study focuses on obtaining an empirical relationship to determine the head between the tundish and the mold, based on pressure measurements in the submerged entry nozzle using full-scale water model experiments. Besides, the energy efficiency to create the swirling flow was investigated using the empirical equation from the results of a water model experiment and a numerical analysis of the swirling flow in the nozzle.

2. Experimental Method

Figure 1 shows a schematic diagram of the full-scale water model equipment used to measure the pressure loss in the submerged entry nozzle. The method of pressure measurement is schematically shown in **Fig. 2**.

The measured pressure loss includes all pressure losses between the measuring points, including loss due to the creation of swirling flow in the nozzle, outlet loss at the outlet port of the nozzle, and so on.

When Bernoulli's equation was applied to the conditions in Fig. 2, the following equation for the head between the tundish and the mold was obtained:

$$H = \frac{P_s - P_m}{\rho_w \cdot g} + \frac{V_s^2}{2g} + \Delta Z \quad \text{.....(1)}$$

where P_m is the pressure at the measuring point, ρ_w is the density of the water, g is the gravitational acceleration, V_s is the mean velocity at the point S, and ΔZ is the axial distance between the positions used for pressure measurements. The velocity at the measurement point M is assumed to be zero and V_s is the mean velocity obtained from the nozzle inner diameter and the flow rate, Q. P_s is the pressure at the position marked in Fig. 2 and can be expressed as:

$$P_s = P_m + (\rho_{Hg} - \rho_w) g h_{Hg} - \rho_w g \Delta z \quad \text{.....(2)}$$

where ρ_{Hg} is the density of mercury and h_{Hg} is the difference of height of the mercury in the manometer.

Seven types of nozzle configuration were tested in water model experiments, as illustrated in **Table 1**. In six cases of the configurations, swirl blades of different lengths and diameters were tested. In addition, a conventional nozzle was included in the test as a reference for the currently used conditions. A schematic diagram of a swirl blade is shown in **Fig. 3**, to illustrate the length in the axial direction, L, the diameter, D_1, and the twist angle, θ. As shown in Table 1, the six different types of nozzles were prepared by modifying the contraction diameter, D_2, downstream from the swirl blade, the twist ratio of the swirl blade, R_T, and the twist angle, θ. In addition, the thickness of the swirl blades varied as follows for the swirling flow nozzle configurations:

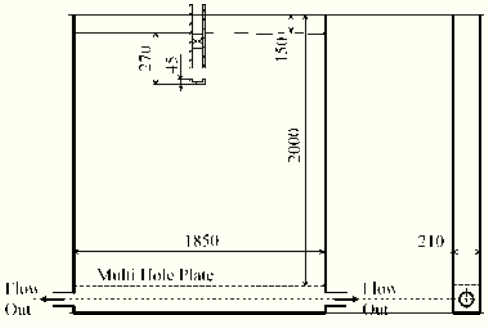

Fig. 1. Schematic geometry of water model set-up.

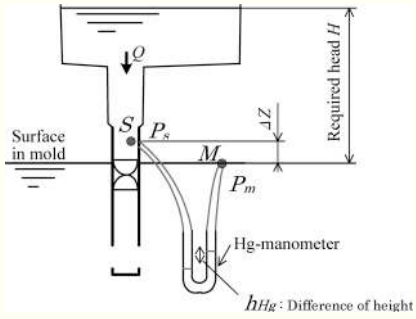

Fig. 2. Experimental set-up to measure head.

Table 1. Specifications of submerged entry nozzles.

	D_1	D_2	L	θ	R_T	Outlet port (W×H)
Swirl-1 (SW1)	85	50	85	180°	1.0	55×60
Swirl-2 (SW2)	85	82	85	180°	1.0	55×60
Swirl-3 (SW3)	85	82	128	180	1.5	55×60
Swirl-4 (SW4)	85	82	85	120	1.5	55×60
Swirl-5 (SW5)	100	82	150	180	1.5	55×90
Swirl-6 (SW6)	100	82	100	120°	1.5	55×90
Conventional	85	82	–	–	–	55×60

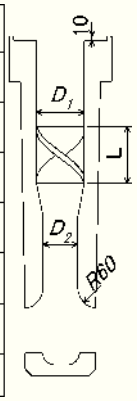

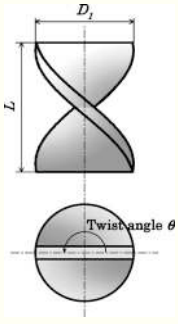

Fig. 3. Dimensions of swirl blade.

20 mm for SW1 to SW4, 14 mm for SW5, and 12.5 mm for SW6. The conventional nozzle without a swirl blade had the same dimensions of main body as nozzle type SW2.

The twist ratio is defined as the length of the swirl blade in the axial direction twisted by 180° divided by the diameter D_1 of the swirl blade as shown in the following equation:

$$R_T = \frac{\pi \cdot L}{\theta \cdot D_1} \quad \text{.....(3)}$$

The total lengths of the nozzles varied between 645 and 730 mm. The length of upper section of the nozzles from the top of the nozzle to the upstream end of the swirl blade varied between 195 and 340 mm. The length of lower section of the nozzles from the downstream end of the nozzle to the downstream end of the outlet varied between 25 and 45 mm. During the trials, an immersion depth of 270 mm from the meniscus to the downstream end of the nozzle was used. The flow rates of water were varied between 0.91×10^{-2} and 1.30×10^{-2} m^3/s, which corresponds to flow rates of 4.2 to 6.1 t/min for molten steel. It should be noted that restrictions such as a sliding gate were not taken into account at the entrance of the nozzle.

The measurement point P_S was set at a diameter of 107 mm in the axial position 110 mm upstream from the upstream end of the nozzle set plate (refer to **Fig. 4**).

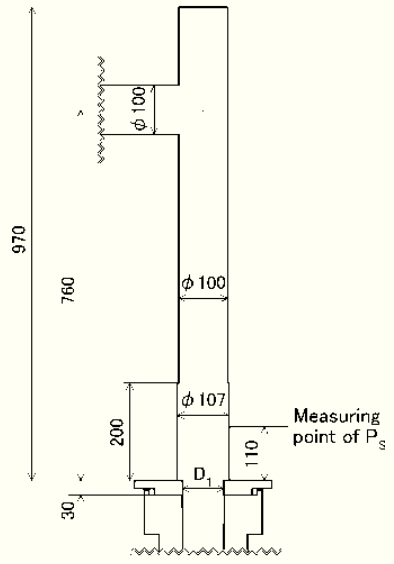

Fig. 4. Schematic geometry of water supply.

3. Results

The aim of the study was to determine the head between the tundish and the mold to optimize swirling flows in submerged entry nozzles equipped with swirl blades. Initially, full-scale water model experiments were done to measure the head. Thereafter, the experimental results were used to obtain an empirical relationship to determine the head.

3.1. Physical Modeling

Full-scale water model experiments were conducted using the experimental procedure described above and the nozzle configurations given in Table 1. The head was measured as illustrated in Fig. 2. The results of measurements of the head are summarized in **Table 2**. The head increased with flow rate in all experiments. The highest head was obtained with the nozzle type of SW1.

Table 2. Heads measured in water model.

Nozzle type	Water flow rate Q ($\times10^{-2}$ m^3/s)			
	0.91	1.04	1.17	1.30
SW1	2.27 m	2.98 m	3.78 m	4.74 m
SW2	1.31 m	1.64 m	2.05 m	2.51 m
SW3	0.80 m	0.99 m	1.22 m	1.53 m
SW4	0.76 m	0.99 m	1.22 m	1.58 m
SW5	–	0.30 m	–	0.54 m
SW6	–	0.36 m	–	–
Conventional	0.43 m	0.57 m	0.72 m	0.88 m

3.2. Derivation of Empirical Equation

When using a swirl blade in a submerged entry nozzle, it would be useful to have access to an empirical relationship instead of needing to perform full-scale physical modeling trials each time the nozzle configuration is changed. Such an equation is derived by using the multiple regression method. The derivation is based on the inner shape of the nozzle and the flow rate through the nozzle as input parameters, since this is convenient from a practical viewpoint.

3.2.1. Selection of Governing Parameters

The heads shown in Table 2 represent total losses ($H_S+H_P+H_C$) between the pressure measurement points.

The factors that have an influence on the total loss are thought to be the following: (1) H_S: loss due to the creation of the swirling flow; and (2) H_P: loss due to changes in flow direction and discharge of flow at the outlet port of the nozzle. It should be noted that the friction loss in the nozzle was inferred to be less than 0.05 m of the measured head, so the influence of friction on the total loss was neglected.

3.2.2. Loss Due to Creation of Swirling Flow

The head loss due to the creation of swirling flow, H_S, is divided into two types: creation of rotational movement and friction loss. In the derivation of the empirical relationship, the swirling flow is assumed to be a forced vortex for the tangential velocity, which is assumed to be proportional to the radius. In addition, all pressure losses related to the creation of a swirling flow are assumed to be proportional to square of the angular velocity of forced vortex. If the angular velocity of the swirling flow can be described using the inner shape of the submerged entry nozzle and the flow rate, square of the described angular velocity with a coefficient can be incorporated into the empirical equation as the H_S term.

The geometric relationship of the velocity along the circumferential part of the swirl blade shown in Fig. 3 is as shown in **Fig. 5**. It is assumed that the ratio of the peripheral tangential velocity to the downward velocity equals the ratio of the peripheral length of the blade, twisted by 180°, to the blade length in the axial direction, twisted by 180°, as shown in Fig. 5. The circumferential velocity is represented

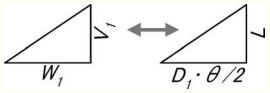

Fig. 5. Geometric relationship of velocity formed along circumferential part of swirling blade.

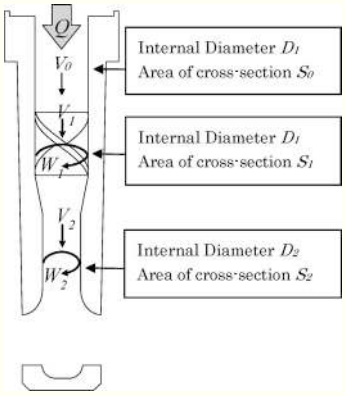

Fig. 6. Dimensions of swirling flow nozzle.

in the following equation using the relationship shown in Fig. 5 and the efficiency coefficient, α:

$$\frac{W_1}{V_1} = \alpha \frac{D_1 \cdot \theta}{2L} \quad \text{.....(4)}$$

where W_1 and V_1 are the tangential and vertical velocities respectively, at the position where the swirl blade is mounted in the nozzle (**Fig. 6**). In the case of ideal swirling flow formation (*i.e.* the ratio of W_1 to V_1 perfectly follows the peripheral inclination of the swirl blade), α becomes 1.0. In other words, in the case of swirling flow formation, α is within the range of $0<\alpha<1.0$.

The law of conservation of angular momentum may be expressed as:

$$W_1 \cdot D_1 = W_2 \cdot D_2 \quad \text{.....(5)}$$

where W_2 is the tangential velocity and D_2 is the inner diameter near the nozzle outlet (Fig. 6). If we thereafter assume that we have an incompressible fluid, the flow rate, Q, can be expressed by the following equation:

$$Q = V_1 \cdot S_1 \quad \text{.....(6)}$$

where S_1 is the cross-section at the position where the swirl blade is mounted in Fig. 6. If Eqs. (3) to (6) are combined, the tangential velocity, W_2, can be expressed as:

$$W_2 = \alpha \frac{\pi \cdot D_1 \cdot Q}{2R_T \cdot S_1 \cdot D_2} \quad \text{.....(7)}$$

The loss of head due to the creation of swirling flow can be determined as follows, if it is assumed that α is constant and does not depend on the inner shape of the nozzle:

$$H_s \propto W_2^2 \propto \left(\frac{W_2}{\alpha}\right)^2 = \left(\frac{\pi \cdot D_1 \cdot Q}{2R_T \cdot S_1 \cdot D_2}\right)^2 \quad \text{.....(8)}$$

It should be noted that the proportionality constant in Eq. (8) was obtained by regression when deriving the empirical equation.

3.2.3. Losses Due to Abrupt Change of Flow Direction and Discharge at Nozzle Outlet

The loss of head corresponding to discharge loss, H_p, can be calculated as follows[14]:

$$H_p = \zeta_p \frac{U_{port}^2}{2g} \propto U_{port}^2 = \left(\frac{Q}{S_{port}}\right)^2 \quad \text{.....(9)}$$

where U_{port}, S_{port}, and ζ_p are the mean velocity at the nozzle outlet, the total cross-section of the outlet, and a coefficient of loss at the outlet of the nozzle, respectively.

The mold is large compared with the cross-section of the outlet of the nozzle. In general, for this case, the coefficient of discharge loss, ζ_P, is considered to be 1.[14] However, the coefficient of discharge loss is thought to become greater than 1 because of uneven flow at the outlet of the nozzle and abrupt changes in flow direction.

To obtain the empirical equation, assuming that all of these losses are proportional to the second power of the mean outlet velocity, the coefficient multiplied by the right side of Eq. (9) was recursively derived.

3.2.4. Contraction Loss at Nozzle Entrance

At the inlet of submerged entry nozzle types SW1, SW2, SW3, SW4, and conventional (Table 2), an abrupt contraction in flow occurs due to the change in the inner nozzle diameter from 107 to 85 mm, as shown in Fig. 5. This leads to a head loss due to contraction, H_c. This abrupt contraction loss is generally expressed as follows,[14] if the loss coefficient, ζ_c, is assumed to be 0.15 in the case that the inner diameter contraction ratio is 0.8[14] ($\because 85/107 \fallingdotseq 0.8$):

$$H_c = \zeta_c \frac{V_0^2}{2g} = \zeta_c \frac{8}{g}\left(\frac{Q}{\pi \cdot D_1^2}\right)^2 \quad \text{.....(10)}$$

where V_0 is the mean vertical velocity in the nozzle just before the swirl blade. Note that for nozzle configurations SW5 and SW6 (Table 1), $\zeta_c = 0$.

The head loss H_c due to abrupt contraction in Eq. (10) was applied to nozzle types SW1 to SW4 and conventional as shown in Table 1 as an empirical equation.

3.2.5. Summary Head Calculation

The total head loss, H_{cal}, can be determined if Eqs. (8) to (10) are summarized as follows:

$$H_{cal.} = H_s + H_p + H_c = a\left(\frac{\pi \cdot D_1 \cdot Q}{2R_T \cdot S_1 \cdot D_2}\right)^2 + b \cdot \left(\frac{Q}{S_{port}}\right)^2 + \zeta_C \frac{8}{g}\left(\frac{Q}{\pi \cdot D_1^2}\right)^2 \quad \text{.....(11)}$$

The a and b coefficients can be determined by regression analysis, so that Eq. (11) can be modified as follows:

$$H_{cal.} = Q^2 \left\{ 5.08 \times 10^{-2} \left(\frac{\pi \cdot D_1}{2R_T \cdot S_1 \cdot D_2}\right)^2 + 2.19 \times 10^{-1} (S_{port})^{-2} + \zeta_C \frac{8}{g} (\pi \cdot D_1^2)^{-2} \right\} \quad \text{.....(12)}$$

4. Discussion

To compare the head calculated using the empirical relationship given in Eq. (12) with experimental data, the measured head data from Table 2 were plotted *versus* the predicted values, as shown in **Fig. 7**. The agreement between the predictions and the measurements was very good, as shown by the R^2 value of 0.994. It should be noted that the agreement was good independent of the different nozzle configurations (Table 2). Thus, it can be concluded that it is possible to derive an empirical relationship that can successfully predict the head between the tundish and the nozzle.

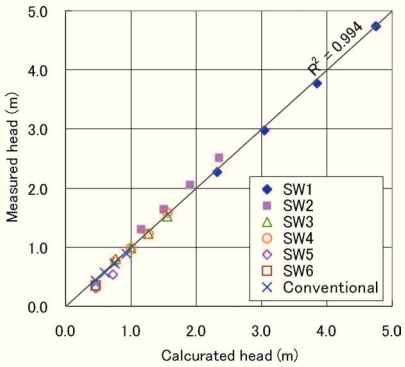

Fig. 7. Comparison of calculated and measured heads.

4.1. Contribution of Each Term in the Empirical Equation

It is of interest to discuss the contribution of each term in Eq. (12). Comparisons were made for a flow rate of 1.04×10^{-2} m^3/s. The calculated heads for each nozzle configuration and each term in Eq. (12) are shown in **Fig. 8**. For the case with a smaller twist ratio of the swirl blade and a smaller contraction diameter downstream from the swirl blade, such as SW1, the most important contribution was found to be made by the first term in Eq. (12). The calculated head for nozzle type SW1 is 3 m, which seems unrealistic for this flow rate because this is bigger than the actual head of general continuous casting machines. However, if the swirling flow nozzle is to be used under a low flow rate condition, such as in billet continuous casting, it is better to use a specification such as SW1, because the head between the tundish and the mold is utilized effectively.

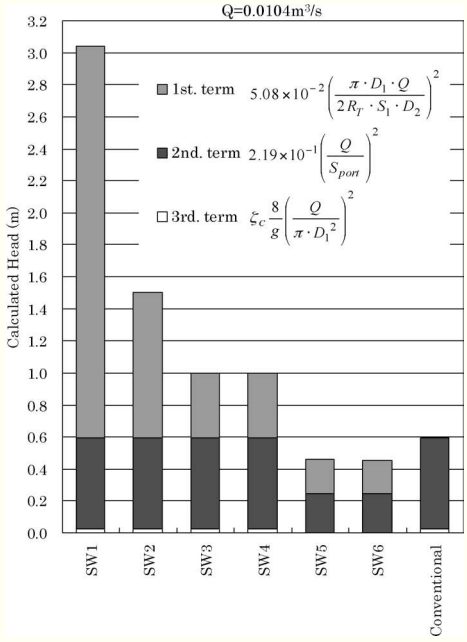

Fig. 8. Influence of each term in Eq. (12) on the prediction of the head.

Figure 8 also shows that the magnitude of the first term decreases to that of the second term for nozzle configurations SW3 to SW6, and the head becomes a reasonable size. In the case of nozzles with comparatively enlarged inner diameters, such as SW5 and SW6, the head is decreased to the same magnitude as that of the conventional nozzle. Thus, nozzle types SW5 and SW6 can be easily applied in the condition of flow rate around 1.04×10^{-2} m^3/s without a problem of deficient head between the tundish and the mold.

Figure 8 shows that the effect of contraction of the inner nozzle diameter from 107 to 85 mm is very small compared with that of other factors such as the first and second terms of Eq. (12). Thus, Eq. (12) may be rewritten as follows:

$$H_{cal.}=Q^2\left\{5.08\times10^{-2}\left(\frac{\pi\cdot D_1}{2R_T\cdot S_1\cdot D_2}\right)^2+2.19\times10^{-1}(S_{port})^{-2}\right\} \quad \text{.....(13)}$$

4.2. Loss at Outlet

The second term in Eq. (12) represents all losses around the outlet of the submerged entry nozzle, including loss due to abrupt changes in flow direction, discharge, and so on, where the coefficient b is derived on the assumption that the consumed head is proportional to the second power of the mean outlet velocity. The coefficient of loss derived from comparison between the second terms of Eqs. (12) and (9) was $\zeta_p=4.3$ ($\because H_P=\zeta_p\cdot U_{port}^2/2g=2.19\times10^{-1}U_{port}^2$). Issues such uneven outlet velocity, formation of flow pattern in the mold, abrupt changes of flow direction near the bottom of the nozzle, and the negligence of friction loss in the nozzle result in a large coefficient of loss of $\zeta_p=4.3$ derived by the superimposed regression method.

Despite such a large coefficient, the empirical equation reproduces the experimental results well because most of the superimposed losses are thought to be losses around the outlet of the nozzle; that is, the losses are proportional to the second power of the mean outlet velocity.

4.3. Energy Efficiency of Creating Swirling Flow

4.3.1. Numerical Analysis of Flow in Nozzle

Deriving the coefficient α in Eq. (7) enables estimation of the energy efficiency of creating a swirling flow compared with the rotational kinetic energy in the first term in Eq. (12). First, the flow pattern in the water model was calculated by three-dimensional numerical analysis. Fluent 6.0[15] was used for the calculations. The Reynolds stress model was used to calculate the turbulent flow due to the swirling flow. The discrete QUICK scheme was also used in the calculations. The boundary conditions were set as fol-

lows: a uniform velocity at the entrance of the submerged entry nozzle, a constant pressure at the outlet of the mold, a slip flow on the meniscus, and a wall function near the wall to account for velocities at the wall.

Calculations were performed for nozzle type SW6 using an entrance flow rate of $Q=1.04\times10^{-2}\,m^3/s$. The calculated contours of the flow velocity at various cross-sections in the nozzle are shown in **Fig. 9**. It is observed that a double helical flow is created from the two flow paths that are formed as the fluid passes the swirl blade. This results in the formation of mainstream regions of double helical flow in the region below the swirl blade. In Fig. 9, the arrowed points are the center of each mainstream region where maximal flow velocity is observed. Minimal flow velocity is observed in the center of each weak-flow region, approximately 90° in the tangential flow direction from each center of the mainstream regions.

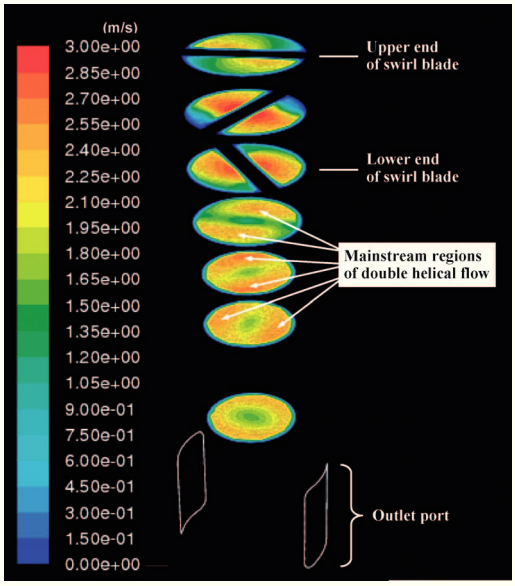

Fig. 9. Contours of flow velocity magnitude in swirling flow nozzle (SW6).

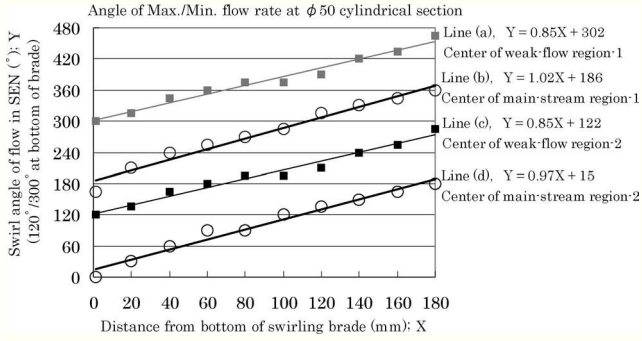

Fig. 10. Swirl angle of flow in submerged entry nozzle as a function of distance from the bottom of the swirl blade.

Scanning the maximal and minimal velocity positions on various circular sections of diameter 50 mm downstream from the exit of the swirl blade revealed relationships between the distance from the bottom of the swirl blade and the swirling angle of flow, as shown in **Fig. 10**. Line (b) and (d) show the rotational angle of each mainstream region along with the nozzle length. In the same manner, line (a) and (c) show the rotational angle of each weak-flow region. From the mean gradient of 0.923°/mm (average gradient of each regression line; (a) 0.85 (b) 1.02, (c) 0.85, (d) 0.97), it was observed that the flow in the nozzle turned with a swirling angle of 923°/m, namely $\beta=5.13\pi$ rad per meter downward distance, downstream from the lower end of the swirl blade. The flowing-downward velocity is expressed by $V_2=4Q/(\pi D_2^2)$, where Q is the flow rate and the D_2 is inner diameter.

The peripheral tangential velocity in the case of a forced vortex being $W_{2act.}=(D_2/2)\cdot\beta\cdot V_2$ ($\because W_{2act.}/V_2=(D_2/2)\cdot\beta$; the same relationship as Fig. 5, here β corresponds to θ/L) yields:

$$W_{2act.}=\frac{2\beta\cdot Q}{\pi\cdot D_2} \quad \text{.....(14)}$$

When W_2 in Eq. (7) and $W_{2act.}$ in Eq. (14) are assumed to be equal, the coefficient $\alpha=4R_T\cdot S_1\cdot\beta/(\pi^2\cdot D_1)$ is obtained. If the shape of nozzle type SW6 ($R_T=1.5$, $S_1=0.006607\,m^2$, $D_1=0.100\,m$, and $\beta=5.13\pi$ rad/m) are inserted into Eq. (14), the coefficient α can be calculated to be 0.65.

4.3.2. Water Model Experiment

The flow pattern was investigated using a transparent acrylic resin nozzle as shown in **Fig. 11**. Measurements were made at the cross-section 160 mm below the downstream end of the swirl blade, and at radial positions of $r=0$ to $r=35$ mm for angle positions from $\gamma=0°$ to $\gamma=-315°$. The tangential angle γ in the swirling direction was defined as positive. The swirl blade had a thickness of 10 mm and a twist angle of 180°. Velocity measurements in the downward and tangential components were made at the same time using a laser Doppler velocimeter, with a flow rate of $Q=1.037\times10^{-2}\,m^3/s$ (622 L/min). The combined velocity of downward and tangential flow at a concentric circle of half of the diameter of the nozzle *versus* the angle γ are shown in **Fig. 12**. Values of angle γ corresponding to the maximal flow velocity on the two regression curves shown in Fig. 12 were −89°, and −261° respectively.

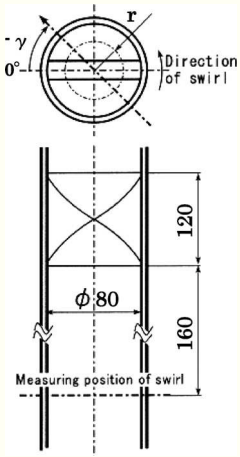

Fig. 11. Schematic view of position of measurement of swirl in submerged entry nozzle.

Considering that the mainstream regions of double helical flow at the exit of the swirl blade (*i.e.* the regions of maximal flow velocity) were in the center parts of

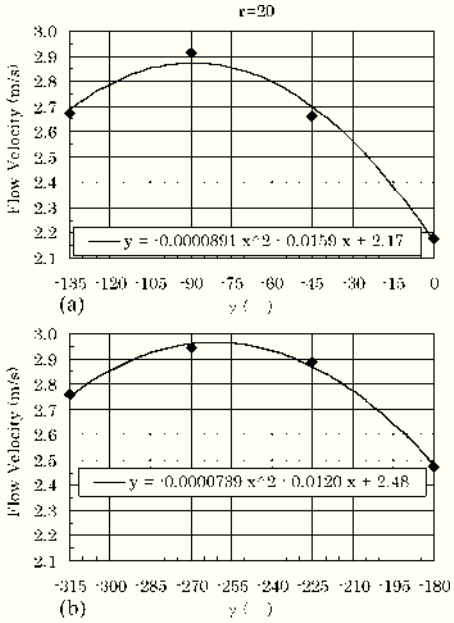

Fig. 12. Relationship between flow velocity in nozzle and tangential position γ.

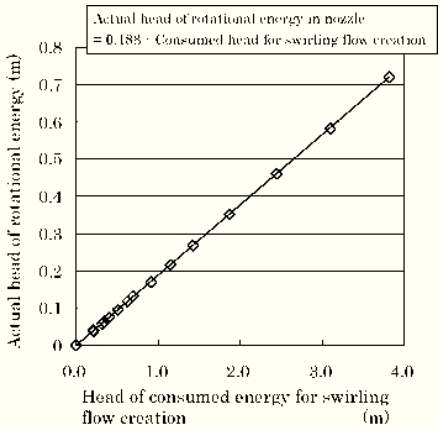

Fig. 13. Comparison of head of rotational energy and head consumed by creation of swirling flow.

the cross-section of the paths, in this case, at $\gamma = -270°$ ($-90° - 180°$) and $-450°$ ($-90° - 180° - 180°$), the swirling flow turns by 181° ($-270°$ to $-89°$) and 189° ($-450°$ to $-261°$) during the distance of downstream from the exit of the swirl blade (refer to Fig. 11). The mean value of 185° was adopted as the turning angle of the double helical flow during 160 mm. That is, the turning angle per meter downward distance is 6.42π rad. If a swirl blade of the shape shown in Fig. 11 is adopted, then Eqs. (7) and (14) are combined using a value of 6.42π rad/m for β, a value of 0.65 for α is obtained. This is the same value as was derived based on mathematical modeling.

4.3.3. Energy Efficiency

As the values for the coefficient α derived by two different methods agreed well with each other, the rotational kinetic energy in the nozzle can be calculated accurately using α.

In a forced vortex, the mean tangential velocity across the nozzle being regarded as $(2/3)W_2$ (∵Integrated tangential velocity over the whole circular cross-section divided by area of circular cross-section is equal to $(2/3)W_2$ in the case that the tangential velocity is proportional to radial position), the rotational kinetic energy, H_r, is given by the following equation:

$$H_r = \frac{\left(\frac{2}{3}W_2\right)^2}{2g} = \frac{2W_2^2}{9g} \quad \text{.....(15)}$$

where W_2 is the peripheral tangential velocity in the nozzle.

The relationship between the rotational kinetic energy in the nozzle through the combination of Eqs. (7) and (15) using α=0.65 and the first term of Eq. (12) (*i.e.* the head consumed by the creation of rotational kinetic energy) is shown in **Fig. 13**. *Hr* in Eq. (15)=0.188×dissipated head of the first term in Eq. (12). Accordingly, the rotational kinetic energy is equal to 18.8% of the head consumed by the creation of swirling flow. The low energy efficiency of the creation of swirling flow suggests that a large pressure loss occurred through the swirl blade under the high velocity flow in the nozzle.

5. Conclusions

Using six kinds of swirling submerged entry nozzle and one conventional submerged entry nozzle in full-scale water model experiments, the required heads between the tundish and the mold were measured.

An empirical equation that gave the necessary head between the tundish and the mold was derived from the shape of the submerged entry nozzle considering the swirl blade and the flow rate in the submerged entry nozzle.

According to the obtained empirical equation, the main heads consumed in the swirling flow submerged entry nozzle are thought to be as follows: (1) the head consumed by the creation of swirling flow and other losses through the swirl blade; and (2) the head consumed around the outlet of the submerged entry nozzle.

Based on the obtained empirical equation, the water model experiment and the numerical analysis, the energy efficiency of creating swirl was found to be approximately 20%.

The obtained empirical equation is useful in designing swirling flow nozzles for various casting conditions.

Acknowledgements

Two authors (Yokoya and Jönsson) wish to thank the Kami Research Foundation for financial support to write this paper.

Nomenclature

H: Required head between tundish and mold (m)
H_s: Head consumed by creating swirling flow (m)
H_p: Head consumed at outlet (m)
H_c: Head consumed by entrance contraction (m)
Q: Flow rate (m^3/s)
P: Pressure (Pa)
U: Velocity (m/s)
V: Vertical velocity (m/s)
W: Tangential velocity (m/s)

Z: Vertical distance (m)
D_1: Inner diameter of immersion nozzle at region with swirl blade, Diameter of swirl blade
D_2: Inner diameter of immersion nozzle between swirl blade and upstream end of outlet of immersion nozzle (m)
L: Length of swirl blade in axial direction (m)
θ: Twist angle of swirl blade (rad)
R_T: Twist ratio of swirl blade (−)
S: Cross-sectional area (m^2)
S_{port}: Total area of outlet (m^2)
ρ: Density (kg/m^3)
g: Acceleration due to gravity (m/s^2)
a: Coefficient (−)
b: Coefficient (−)
α: Coefficient (−)
β: Turning angle with flowing-downward distance (rad/m)

REFERENCES

1) T. Tokonami, Y. Ogami, K. Matuo, Y. Tai, M. Morisita, H. Yasunaka and K. Ayata: *CAMP-ISIJ*, **9** (1996), 606.
2) Y. Ohtani, J. Fukuda, A. Kiyose, T. Kawase, J. Nakashima and K. Nakamura: Proc. of 1st. Int. Cong. on Science and Tech. of Steelmaking (ICS '96), ISIJ, Tokyo, Japan, (1996), 97.
3) M. Iguchi, J. Yoshida, T. Shimizu and Y. Mizuno: *ISIJ Int.*, **40** (2000), 685.
4) K. Suzuki, K. Murata, K. Nakanisi, M. Kodama, S. Kozima and Y. Miyazaki: *Tetsu-to-Hagané*, **68** (1982), S920.
5) S. Idokawa, Y. Kitano and K. Tozawa: *Kawasaki Steel Tech. Rep.*, **28** (1996), 46.
6) W. Yamada, A. Kiyose, J. Nakashima, A. Fukuda, K. Okazawa and K. Miyazawa: *CAMP-ISIJ*, **12** (1999), 682.
7) J. Kubota, N. Kubota, M. Suzuki, T. Ishii, R. Nishimachi and N. Aramaki: *Tetsu-to-Hagané*, **86** (2000), 271.
8) S. Yokoya, S. Takagi, M. Iguchi, Y. Asano, R. Westoff and S. Hara: *ISIJ Int.*, **38** (1998), 827.
9) S. Yokoya, S. Takagi, M. Iguchi, K. Marukawa, W. Yasugaira and S. Hara: *ISIJ Int.*, **40** (2000), 584.
10) S. Yokoya, R. Westhoff, Y. Asako, S. Hara and J. Szekely: *Tetsu-to-Hagané*, **80** (1994), 759.
11) Y. Tsukaguchi, S. Furuhashi and M. Kawamoto: *ISIJ Int.*, **44** (2004), 350.
12) Y. Tsukaguchi, T. Watanabe, S. Yokoya, S. Hara, K. Marukawa and K. Nonobe: *CAMP-ISIJ*, **15** (2002), 839.
13) S. Kosaka, M. Yoshihara, H. Hayashi, K. Iwata, Y. Tsukaguchi and S. Yokoya: *CAMP-ISIJ*, **16** (2003), 949.
14) S. Furuya, M. Murakami and Y. Yamada: Kaitei-shinban-Ryutaikougaku, Asakura-shoten, Tokyo, (1984), 125.
15) FLUENT 6.0 User's Guide, ed. by Fluent Inc., (2001).